Journal of Materials Chemistry A

Accepted Manuscript

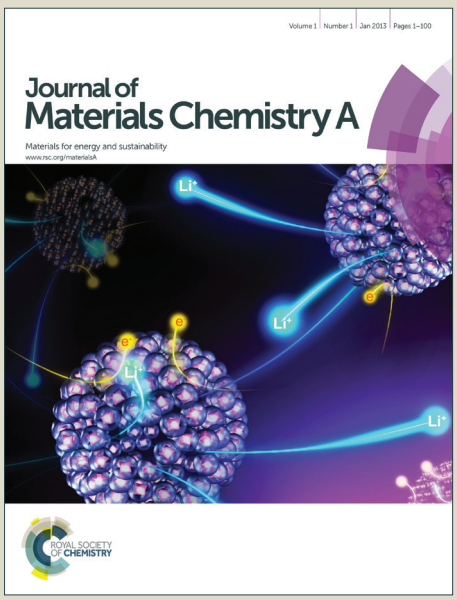

ROYAL SOCIETY OF CHEMISTRY

www.rsc.org/materialsA

Journal Name

COMMUNICATION

Large-scale aligned crystalline $CH_3NH_3PbI_3$ Perovskite array films

Received 00th January 20xx,
Accepted 00th January 20xx

DOI: 10.1039/x0xx00000x

www.rsc.org/

Yitan Li, [a, b] Xiao Wang,[a] Shiting Wu,[c] Haina Ci, [a, b] Henglu Xu, [a] Xuemei Li,[d] Hao Sun,[e] Zeyao Zhang,[a] Anyuan Cao,[c] Xuefeng Guo, [a, b] and Yan Li [*,a ,b]

Owing to the lattice match, aligned $CH_3NH_3PbI_3$ perovskite array films composed of $CH_3NH_3PbI_3$ microribbons with the length at sub-millimeter scale were fabricated on ST cut quartz which showed fast photo response. This method provides a simple and flexible approach to grow oriented crystalline $CH_3NH_3PbI_3$ arrays at millimeter scale.

Organic-inorganic hybrid lead halide perovskite ($CH_3NH_3PbX_3$, X=Cl, Br, I) based solar cells pioneered by Kojima et al. have obtained a significant improvement in power conversion efficiency from 3.8% to 20.1% in the past five years.[1-22] It is well known that the diffusion length of perovskite layer, which is closely related to the film crystallinity and morphology, plays a key role in performances of the device. Large efforts have been exerted to enhance the photovoltaic performance by improving the crystallinity of $CH_3NH_3PbX_3$ film and therefore increasing the diffusion length.[2,13-17,20,23] Horváth et al first prepared lead iodide perovskite ($CH_3NH_3PbI_3$) nanowires with length up to 10 μm.[24] Shi et al. obtained crack-free $MAPbX_3$ single crystals exceeding 100 mm^3 in volume and observed low trap-state density and large carrier diffusion lengths above 10 μm.[23] Nie et al. reported a solution-processed perovskite solar cells with millimeter-scale grains and recorded efficiencies approaching 18% with little cell-to-cell variability. [20]

Besides the crystallinity, it is known that the organization or the arrangements of the materials is also an important issue. For example, oriented arrays of one-dimensional single crystalline ZnO and TiO_2, compared to random polycrystalline nanostructures, showed longer electron diffusion length and faster charge transport, which provides a solution to further improve the performances of solar devices.[25,26] Yet, till now, there is no any report about the preparation of well-aligned lead halide perovskite crystals.

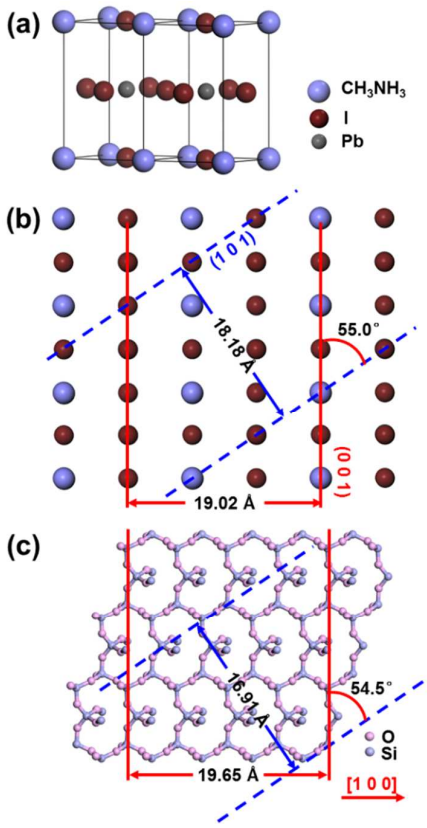

Scheme 1. The structure matching between $CH_3NH_3PbI_3$ and ST cut quartz. (a) Two unit cells of $CH_3NH_3PbI_3$; (b) d_{001} and d_{101} shown on (0 1 0) plane of $CH_3NH_3PbI_3$; (c) Periodical structure on the surface of ST cut quartz.

[a] *Key Laboratory for the Physics and Chemistry of Nanodevices, Beijing National Laboratory of Molecular Sciences, State Key Laboratory of Rare Earth Materials Chemistry and Applications, College of Chemistry and Molecular Engineering, Peking University, Beijing 100871, China*
[b] *Academy for Advanced Interdisciplinary Studies, Peking University, Beijing 100871, China*
[c] *Department of Materials Science and Engineering, Peking University, Beijing 100871, China*
[d] *Electron Microscopy Laboratory, Peking University, Beijing 100871, China*
[e] *Bruker (Beijing) Scientific Technology Co., Ltd., Beijing 100081, China*
Electronic Supplementary Information (ESI) available: [details of any supplementary information available should be included here]. See DOI: 10.1039/x0xx00000x

Epitaxy has shown to be a powerful strategy to prepare ordered crystalline nanostructures of wide variety of materials such as giant magnetoresistance nanostructures, semiconducting thin films, and graphene.[27-31] Lattice match between the substrate and the target material is essential in epitaxial growth. With a suitable substrate, we may be able to epitaxially grow ordered $CH_3NH_3PbX_3$ crystals.

We find that the surface of ST cut quartz, which has been widely used to guide the growth of horizontally aligned single-walled carbon nanotube (SWNT) arrays,[32-35] shows similar structural characteristics to tetragonal $CH_3NH_3PbI_3$ as shown in Scheme 1. Along [1 0 0] direction on the surface of ST cut quartz, which is just the direction SWNT oriented, there is a structural period with the scale of 19.65 Å (l_a). The lattice spacing of (0 0 1) planes of $CH_3NH_3PbI_3$ is 12.68 Å (d_{001}).[1] It can be found that $2l_a \approx 3d_{001}$ with a mismatch of 3.2 %. (1 0 1) plane in $CH_3NH_3PbI_3$, whose dihedral angle with (0 0 1) plane is 55.0°, present the lattice spacing of 7.30 Å (d_{101}). In the surface lattice of ST cut quartz, along the direction of 54.5° apart from [1 0 0], a period of 16.91 Å (l_b) exists. It can also be found that $2l_b \approx 5d_{101}$ with a mismatch of 7.0 %. This length adaption is not perfect but still acceptable. However, the angle mismatch is only 0.9%. Hence, ST cut quartz might be possible to act as the substrate for the epitaxial growth of crystallized $CH_3NH_3PbI_3$ structures relying on the lattice match between the two materials. Also, the surface structure of X, Y, Z cut quartz was also investigated as shown in Figure S1 and the periodic lengths are listed in Table S1. They do not show good structural match to $CH_3NH_3PbI_3$ crystal.

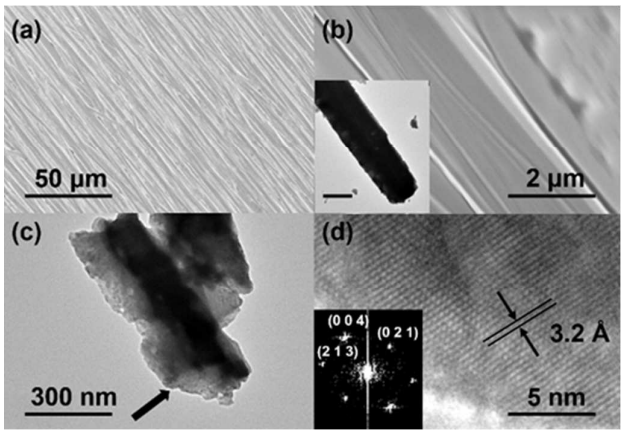

Figure 1. SEM and TEM characterization of $CH_3NH_3PbI_3$ microribbons formed on ST cut quartz. (a, b) Low (a) and high magnification (b) SEM images. Inset shows the TEM image of a single perovskite micro ribbon. The bar represents 2 μm. (c, d) TEM (c) and the HRTEM (d) image of the site pointed by the arrow in (c). The corresponding FFT pattern is inserted in (d).

We tried to use slip-coating[24] method to grow $CH_3NH_3PbI_3$ crystals on ST cut quartz substrate with DMF (N, N-dimethyl formamide) solution and a glass slide as the slip. As shown in Figure 1 a & b, aligned microribbon arrays with the length of hundreds of microns were grown on the surface of ST cut quartz. All peaks in the X-ray diffraction (XRD) pattern of the sample can be readily assigned to tetragonal $CH_3NH_3PbI_3$ and the quartz substrate as shown in Figure S2. The intensive peaks appearing at 2θ of 13.9°, 14.3°, 28.0°, and 28.6° correspond to diffractions of (0 0 2), (1 1 0), (0 0 4), and (2 2 0) planes of $CH_3NH_3PbI_3$, respectively. [1] This indicates that well crystalized perovskite with good phase purity were formed on quartz. High resolution transmission electron microscopy (HRTEM) image in Figure 1d shows fringes perpendicular to the longitudinal direction of the microribbon with the inter-distance of 3.2 Å, which is in good accordance with d_{004} (3.17 Å) of $CH_3NH_3PbI_3$. Fourier transform pattern of the HRTEM image can also be well ascribed to tetragonal $CH_3NH_3PbI_3$. Therefore the microribbons extend along [0 0 1] direction or c axis of $CH_3NH_3PbI_3$ crystal.

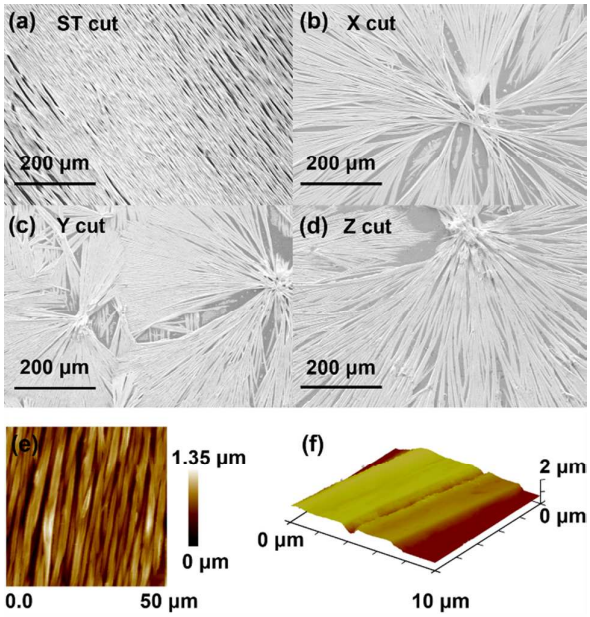

Figure 2. SEM images of $CH_3NH_3PbI_3$ performed on ST (a), X (b), Y (c), Z (d) cut quartz and tapping-mode AFM topographic image (e) as well as 3D height image (f) of the aligned $CH_3NH_3PbI_3$ arrays at different magnifications.

We also performed slip-coating under the same condition on X, Y, and Z cut quartz, respectively. On these quartz substrates, $CH_3NH_3PbI_3$ crystals were randomly oriented (Figure 2b-d). But on ST cut quartz, no matter what directions we moved the slipping slide, the $CH_3NH_3PbI_3$ microribbons were always oriented along the same direction, i. e. 45° to the margins of the quartz substrates as shown in Figure 3. This is the same direction as the aligned SWNT arrays on ST cut quartz and we know it is [1 0 0] direction of quartz.[32, 35] All these facts reveal that the surface lattice of ST cut quartz is responsible for the formation of aligned $CH_3NH_3PbI_3$ ribbons. Taking the HRTEM characterization in Figure 1 into account, it is obvious that the [0 0 1] direction of $CH_3NH_3PbI_3$ parallels to [1 0 0] direction of quartz. This is in good accordance to what we already predicted in Scheme 1.

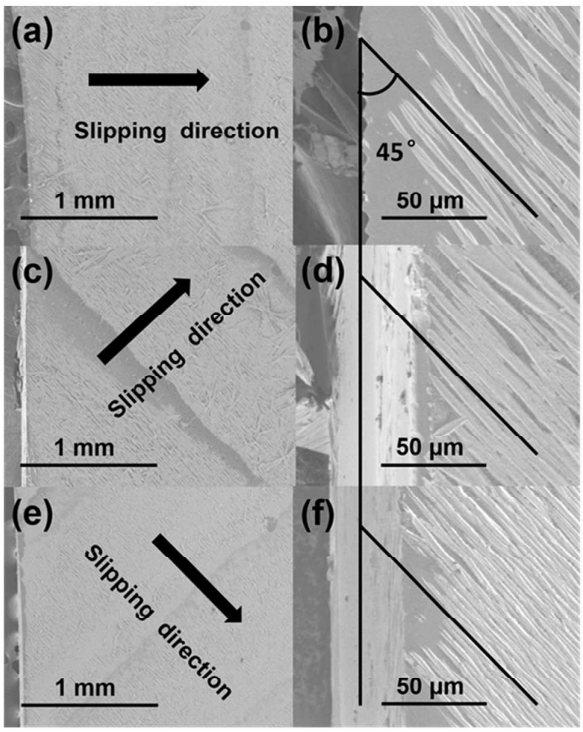

Figure 3. SEM images of $CH_3NH_3PbI_3$ micro ribbons fabricated under different slip-coating directions.

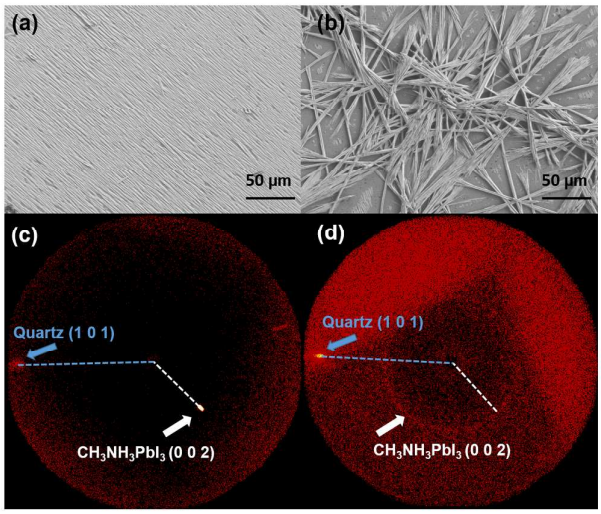

Figure 4. SEM images and 2D WAXD pattern XRD patterns of the substrate with aligned $MAPbI_3$ microribbon arrays (a, c) and $CH_3NH_3PbI_3$ microribbons with disordered orientations (b, d).

We carried out two-dimensional wide angle X-ray diffraction (WAXD) measurements at the 2θ range of 0 to 30° to further verify the structural correlation between $CH_3NH_3PbI_3$ microribbons and the ST cut quartz. In the two-dimensional WAXD images, 2θ is represented by the distance to the center. Blank ST cut quartz only shows one diffraction spot at 2θ of ~26.6° (Figure S3), which was assigned to (1 0 1) planes of ST cut quartz (JCPDS no. 46-1045). This spot also appears in the diffraction patterns of ST cut quartz substrates with $CH_3NH_3PbI_3$ microribbons (Figure 4c & d). $CH_3NH_3PbI_3$ microribbon arrays presents a strong diffraction spot at ~ 13.9° (Figure 4c); while disordered $CH_3NH_3PbI_3$ microribbons only show a weak ring at the same diffraction angle (Figure 4d), which corresponds to (0 0 2) planes of $CH_3NH_3PbI_3$. This result indicates the well alignment of $CH_3NH_3PbI_3$ microribbon arrays made by slip-coating method. In WAXD patterns, the angle between (0 0 2) plane of $CH_3NH_3PbI_3$ and (1 0 1) plane of ST cut quartz is about 43.0°. We know that the angle between (1 0 1) planes and (1 0 0) planes of ST cut quartz is ~42.3°. Therefore, c axis of $CH_3NH_3PbI_3$ microribbons is parallel to [1 0 0] direction of quartz. The WAXD measurements reveal the orientation of $CH_3NH_3PbI_3$ crystal on ST cut quartz and provides further evidence for the epitaxial growth mechanism.

The thickness of the liquid films on the quartz substrate can be varied by changing the pressure exerted onto the slipping slide, subsequently the thickness of the $CH_3NH_3PbI_3$ microribbons can be easily adjusted. As shown in Figure S4, the average heights have been modulated from ~ 400 nm to ~ 2 μm, though some sophisticated techniques are needed to realize a precise control. Figure 2e & f shows the typical AFM images of the $CH_3NH_3PbI_3$ microribbon arrays with the thickness of ~ 700 nm. The widths of the ribbons are around hundreds of nanometers to several microns.

Because the $CH_3NH_3PbI_3$ microribbons were formed on quartz, the samples are ready for direct detection of the UV-Vis-NIR absorption. The microribbons show intensive and broad absorption from UV to near IR region till ~ 800 nm as shown in Figure S6. The bandgap was estimated to be ~1.6 eV, which is very similar to the reported values.[1, 4]

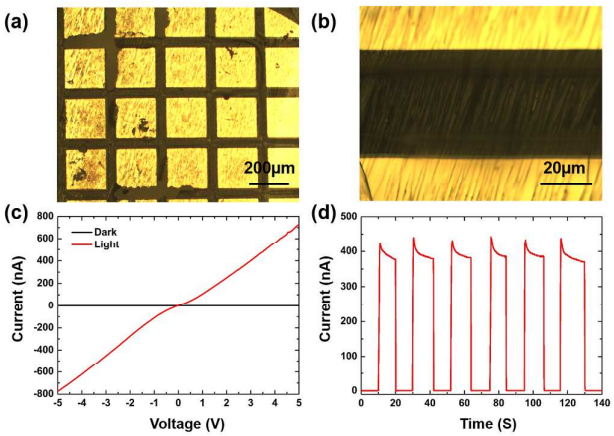

Figure 5. The devices of $CH_3NH_3PbI_3$ microribbon arrays with Au as electrodes and the photo response performance. (a, b) Images of the devices with the electrodes at low and high amplifications; (c, d) I–V (c) and I-T (d) characteristics of devices.

Au electrodes with thickness of 60 nm and 8 nm of Cr buffer layer was evaporated directly onto the quartz substrates with $CH_3NH_3PbI_3$ microribbons to fabricate devices and their photo response performances were studied (Figure 5). The channel lengths between two electrodes are about 40 μm and the side length of the square Au electrodes are ~ 200μm. We measured the I-T curves under an ON/OFF interval of ~ 10 s. The response time of

the photocurrent was observed to be ~ 0.1 s, which actually already reaches the limitation of our detector. The photo current of devices built on aligned microribbons is normally 5 times higher than the device of disordered $CH_3NH_3PbI_3$ microribbons (Figure S5). In addition, sample annealed under 80 °C for 2 hours was measured for comparison. No obvious difference in photo response performance was observed. This may indicate that $MAPbI_3$ microribbons formed by epitaxial growth are already with considerable crystallinity.

Conclusions

In summary, aligned $CH_3NH_3PbI_3$ array films with high-quality crystallization have been fabricated on ST cut quartz via a slip-coating method. The surface lattice of ST cut quartz acts as the template to guide the epitaxial growth of $CH_3NH_3PbI_3$ microribbon arrays. The matching between the lattice spacing of (0 0 1) planes of $CH_3NH_3PbI_3$ and the intervals along [1 0 0] direction of ST cut quartz leads to the oriented growth of $CH_3NH_3PbI_3$ microcrystals along [1 0 0] direction of ST cut quartz, resulting in $CH_3NH_3PbI_3$ microribbons extended along *c* axis. These ribbons are at the length of sub-millimeter scale, width of microns, and thickness of hundreds of nanometers to several microns depending on the preparation conditions. The elimination of grain boundaries is always desired for perovskite-based devices. The epitaxial growth on ST cut quartz obtains a strategy to produce large scale aligned microribbon perovskite films with high crystallinity, which may bring about improved performance. In addition, the alignment of the microribbons should lead to heterogeneous performance along different directions, which can also be made use of in certain applications.

ACKNOWLEDGMENT

We thank Prof. X. Jing for discussion in crystal structure and Prof. S. Wang for the help in device measurements. This work is supported by Ministry of Science and Technology of China (Project 2011CB933003), the National Natural Science Foundation of China (projects 21125103, 91333105, and 21321001).

Notes and references

1 J. H. Im, C. R. Lee, J. W. Lee, S. W. Park and N. G. Park, *Nanoscale*, 2011, **3,** 4088.
2 M. M. Lee, J. Teuscher, T. Miyasaka, T. N. Murakami and H. J. Snaith, *Science*, 2012, **338**, 643–647.
3 Y. X. Zhao and K. Zhu, *J. Am. Chem. Soc.*, 2014, **136**, 12241–12244.
4 L. Etgar, P.Gao, Z. S. Xue, Q. Peng, A. K. Chandiran, B. Liu, M. K. Nazeeruddin and M. Grätzel, *J. Am. Chem. Soc.*, 2012, **134**, 17396–17399.
5 G. Giorgi, J. I. Fujisawa, H. Segawa and K. Yamashita, *J. Phys. Chem. Lett.*, 2013, **4**, 4213–4216.
6 H. J. Snaith, *J. Phys. Chem. Lett.*, 2013, **4**, 3623–363.
7 H. S. Kim, S. H. Im and N. G. Park, *J. Phys. Chem. C*, 2014, **118**, 5615–5625.
8 S. D. Stranks, G. E. Eperon, G. Grancini, C. Menelaou, M. J. P. Alcocer, T. Leijtens, L. M. Herz, A. Petrozza and H. J. Snaith, *Science*, 2013, **342**, 341–344.
9 G. C. Xing, N. Mathews, S. Y. Sun, S. S. Lim, Y. M. Lam, M. Grätzel, S. Mhaisalkar and T. C. Sum, *Science*, 2013, **342**, 344-347.
10 A. Kojima, K. Teshima, Y. Shirai and T. Miyasaka, *J. Am. Chem. Soc.*, 2009, **131**, 6050–6051.
11 B. V. Lotsch, *Angew. Chem. Int. Ed.*, 2014, **53**, 635–637.
12 N. G. Park, *J. Phys. Chem. Lett.*, 2013, **4**, 2423–2429.
13 M. J. Carnie, C. Charbonneau, M. L. Davies, J. Troughton, T. M. Watson, K. Wojciechowski, H. Snaith and D. A. Worsley, *Chem. Commun.*, 2013, **49**, 7893.
14 J. Burschka, N. Pellet, S. J. Moon, R. H. Baker, P. Gao, M. K. Nazeeruddin and M. Grätzel, *Nature*, 2013, **499**, 316–319.
15 D. Y. Liu and T. L. Kelly, *Nat. Photonics*, 2013, **8**, 133–138.
16 M. Z. Liu, M. B. Johnston and H. J. Snaith, *Nature*, 2013, **501**, 395–398.
17 Q. Chen, H. P. Zhou, Z. R. Hong, S. Luo, H. S. Duan, H. H. Wang, Y. S. Liu, G. Li and Y. Yang, *J. Am. Chem. Soc.*, 2014, **136**, 622–625.
18 H. S. Kim, J. W. Lee, N. Yantara, P. P. Boix, S. A. Kulkarni, S. Mhaisalkar, M. Grätzel and N. G. Park, *Nano Lett.*, 2013, **13**, 2412–2417.
19 H. P. Zhou, Q. Chen, G. Li, S. Luo, T. B. Song, H. S. Duan, Z. R. Hong, J. B. You, Y. S. Liu and Y. Yang, *Science*, 2014, **345**, 542–546.
20 W. Y. Nie, H. H. Tsai, R. Asadpour, J. C. Blancon, A. J. Neukirch, G. Gupta, J. J. Crochet, M. Chhowalla, S. Tretiak, M. A. Alam, H. L. Wang and A. D. Mohite, *Science*, 2015, **347**, 522-525.
21 J. H. Im, J. S. Luo, M. Franckevičius, N. Pellet, P. Gao, T. Moehl, S. M. Zakeeruddin, M. K. Nazeeruddin, M. Grätzel and N. G. Park, *Nano Lett.*, 2015, **15**, 2120–2126.
22 W. S, Yang, J. H, Noh, N. J. Jeon, Y. C. Kim, S. C. Ryu, J. W. Seo and S. I. Seok, *Science*, 2015, **348**, 1234-1237.
23 D. Shi, V. Adinolfi, R. Comin, M. J. Yuan, E. Alarousu, A. Buin, Y. Chen, S. Hoogland, A. Rothenberger, K. Katsiev, Y. Losovyj, X. Zhang, P. A. Dowben, O. F. Mohammed, E. H. Sargent and O. M. Bakr, *Science*, 2015, **347**, 519–522.
24 E. Horváth, M. Spina, Z. Szekrényes, K. Kamarás, R. Gaal, D. Gachet and L. Forró, *Nano Lett.*, 2014, **14**, 6761–6766.
25 M. Law, L. E. Greene, J. C. Johnson, R. Saykally and P. D. Yang *Nat. Mater.*, 2005, **4**, 455–459.
26 X. J. Feng, K. Shankar, O. K. Varghese, M. Paulose, T. J. Latempa and C. A. Grimes, *Nano Lett.*, 2008, **8**, 3781–3786.
27 M. N. Baibich, J. M. Broto, A. Fert, F. Nguyen Van Dau and F. Petroff, *Phys. Rev. Lett.*, 1988, **61**, 2472-2475.
28 G. Binasch, P. Grünberg, F. Saurenbach and W. Zinn, *Phys. Rev. B*, 1989, **39**, 4828-4830.
29 C. Berger, Z. M. Song, X. B. Li, X. S. Wu, N. Brown, Cécile Naud, D. Mayou, T. B. Li, J. Hass, A. N. Marchenkov, E. H. Conrad, P. N. First and W. A. de Heer, *Science*, 2006, **312**, 1191–1196.
30 K. V. Emtsev, A. Bostwick, K. Horn, J. Jobst, G. L. Kellogg, L. Ley, J. L. McChesney, T. Ohta, S. A. Reshanov, J. Röhrl, E. Rotenberg, A. K. Schmid, D. Waldmann, H. B. Weber and T. Seyller, *Nat. Mater.*, 2009, **8**, 203–207.
31 H. B. Chu, L. Ding, J. Y. Wang, X. M. Li, L. P. You and Y. Li, *J. Phys. Chem. C*, 2008, **112**, 18938–18942.
32 L. Ding, D. N. Yuan and J. Liu, *J. Am. Chem. Soc.*, 2008, **130**, 5428–5429.
33 J. Liu, C. Wang, X. M. Tu, B. L. Liu, L. Chen, M Zheng and C. W. Zhou, *Nat. Commun.*, 2012, **3**, 1199.
34 S. J. Kang, C. Kocabas, T. Ozel, M. Shim, N. Pimparkar, M. A. Alam, S. V. Rotkin and J. A. Rogers, *Nat. Nanotechnol.*, 2007, **2**, 230–236.
35 J. L. Xiao, S. Dunham, P. Liu, Y. W. Zhang, C. Kocabas, L. Moh, Y. G. Huang, K. C. Hwang, C. Lu, W. Huang and J. A. Rogers, *Nano Lett.*, 2009, **9**, 4311–4319.